Measurement of the neutron flux distribution in a research reactor by neutron activation analysis

Byung-Gun Park[1] [ORCID] · Byung Jin Jun[1] · Gi-Doo Kang[1] · Myong-Seop Kim[1] · Han Jong Yoo[1] · Byun-Young Chung[1] · Byungchul Lee[1]

Abstract
The neutron flux distribution in the core region of the JRTR was measured through the neutron activation analysis method. Sample mount and a tool for withdrawing the sample mount were devised to irradiate the Au wires and foils. The measured data were compared with calculated values to confirm the reliability of the power distribution calculation. The reactor power during irradiation was estimated to be 9% lower than indications of power monitoring systems calibrated at around 10 μW. The measured transversal and axial neutron reaction rate distributions showed agreement within 1.32% difference with the calculated results.

Introduction

Research reactors are used for education and training, materials testing, neutron science, production of radioisotopes for medicine and industry, etc. The primary purpose of a research reactor is to provide a neutron source for research and other purposes. Therefore, the neutron flux is an essential parameter when evaluating the performance of research reactors. Particularly for commissioning of a new research reactor, accurate measurements of the neutron flux are required for verification of the core design, calibration of the fission power, etc.

Usually, neutron flux and neutron energy spectrum measurements require an assortment of neutron activation foils and threshold detectors as well as counting equipment to the level of sophistication desired [1]. However, accurate determination of the neutron flux in the core region of research reactors is difficult due to various perturbations, such as those associated with experimental assemblies, local burn-up and control-rod positions [2]. Given the increase in calculating power, researchers have devised sophisticated

reactor core analysis methods via Monte Carlo simulations and have calculated neutron flux distributions in great detail [3–5]. These studies measured the neutron flux through the neutron activation technique and validated the reliability of calculation. According to these studies, the simulation results predict actual values well, but verification of the simulation data experimentally should also be done when a research reactor newly operates.

The Jordan Research and Training Reactor (JRTR) is an open tank-in-pool type of reactor with 5 MW of thermal power. Various tests were conducted during the reactor commissioning stage in 2016 [6–8]. In this paper, experimental details on the neutron flux distribution in the fuel assemblies of the JRTR during the commissioning test are presented. The purpose of this study is to check the reliability of predictions of the power distribution at an approximate reactor power of 2 kW and to provide basic data for the safe and reliable operation of the reactor.

Neutron flux determination by an activation analysis

The neutron flux distribution in the research reactor was determined by measuring the neutron reaction rate of Au wires and foils. Neutron detection by the activation of Au

✉ Byung-Gun Park
   bgpark@kaeri.re.kr

1   Korea Atomic Energy Research Institute, Daedeok-daero 989-111, Yuseong-gu, Daejeon 34057, South Korea

is based on the formation of the radioisotope Au-198 by (n,γ) neutron capture reactions. The reaction rate R of Au-197 during neutron irradiation in the core is given by

$$R = N_0 \int_0^\infty \phi(E)\sigma(E)\mathrm{d}E, \tag{1}$$

where N_0 is the number of Au-197 nuclides and $\sigma(E)$ is the capture microscopic cross-section of the neutron with energy E. $\phi(E)$ is the neutron flux with energy E, which is considered to be constant in time. As the depletion of Au-197 during the irradiation is negligible in this experiment, the N_0 is assumed constant. In this study, the reaction rates are measured in the cooling channels between fuel plates of the fuel assemblies (FAs), where the neutron spectra are rather hard. The thermal neutron flux was derived from the measured reaction rate and the calculated values. If the number of Au-198 nuclides N is 0 at the beginning of irradiation, at the end of irradiation, it becomes,

$$N(t_i) = e^{-\lambda t_i} \int_0^{t_i} R(t)e^{\lambda t}\mathrm{d}t, \tag{2}$$

where λ is the decay constant of Au-198 (s^{-1}), and t_i is the irradiation time. Then, the activity of Au-198 at the end of the irradiation is determined with the following equation:

$$A(t_i) = R_0(1 - e^{-\lambda t_i}). \tag{3}$$

If gamma-ray counting is carried out over a time interval from $t_i + t_d$ to $t_i + t_f$, the number of gamma rays counted by the detector will be

$$C = \varepsilon p(1 - C_D) \int_{t_d}^{t_f} A(t_i)e^{-\lambda t}\mathrm{d}t + B = \frac{\varepsilon p(1 - C_D)A(t_i)\left(e^{-\lambda t_d} - e^{-\lambda t_f}\right)}{\lambda} + B, \tag{4}$$

where ε is the full-energy photopeak efficiency of the detector, p is the gamma-ray emission probability (photons/disintegration), C_D is the dead time correction factor, and B is the number of background counts. Then, the activity of Au-198 is determined as

$$A(t_i) = \frac{\lambda(C - B)}{\varepsilon p(1 - C_D)\left(e^{-\lambda t_d} - e^{-\lambda t_f}\right)}. \tag{5}$$

The reaction rate R_0 in Eq. (3) can be obtained with $A(t_i)$ from Eq. (5). In this study, the absolute reaction rates of the Au foils and the relative distribution of the Au wire reaction rate were determined. In order to compare the measured relative reaction rate distribution with

the calculated one, the associated normalization factor is required. This can be obtained by fitting an average ratio between the measured relative reaction rates and the calculated reaction rates at a fixed power level. The total reaction rate R_0 consists of the thermal and non-thermal reaction rates as given by

$$R_0 = G_{th}N_0 \int_0^{0.625\,\mathrm{eV}} \phi(E)\sigma(E)\mathrm{d}E + G_{nth}N_0 \int_{0.625\,\mathrm{eV}}^\infty \phi(E)\sigma(E)\mathrm{d}E = R_{th} + R_{nth}, \tag{6}$$

where G_{th} and G_{nth} are the self-shielding factors for the thermal neutron and the non-thermal neutron of Au-197, respectively, and R_{th} and R_{nth} are the thermal neutron reaction rate and the non-thermal neutron reaction rate, respectively. If the thermal to total reaction rate ratio F from the core calculation is used, the thermal neutron reaction rate can be obtained as follows:

$$R_{th} = R_0 F \tag{7}$$

The thermal neutron flux is defined as an integral over the thermal energy levels of the neutron spectrum, and the thermal neutron reaction rate R_{th} is expressed as a product of the thermal neutron flux and the average thermal neutron cross-section:

$$\phi_{th} = \int_0^{0.625\,\mathrm{eV}} \phi(E)\mathrm{d}E = \frac{R_{th}}{N_0\, \bar{\sigma}_{th}}, \tag{8}$$

where $\bar{\sigma}_{th}$ is the average thermal neutron cross-section of Au-197 obtained from the core calculation. The thermal neutron flux ϕ_{th} can be derived from the measured reaction rate by Eq. (8).

Experimental

Sample preparation

The JRTR core consists of plate-type fuel assemblies (FAs) of all identical geometry, and a FA has 21 low enriched uranium (LEU) fuel plates [9]. The thickness of the coolant channel between adjacent fuel plates is 2.35 mm. To install the Au wire and foils at the coolant channel, a detector mount was designed, as shown in Fig. 1. It consists of two 1 mm thick polycarbonate (PC) plates to fix a long Au wire and foils in between them, and has two legs. The Au wire used to measure the axial neutron flux distribution at the

Fig. 1 Detector mount used to attach the Au wire and foils, and inserted into the coolant channels of the fuel assembly (unit: mm)
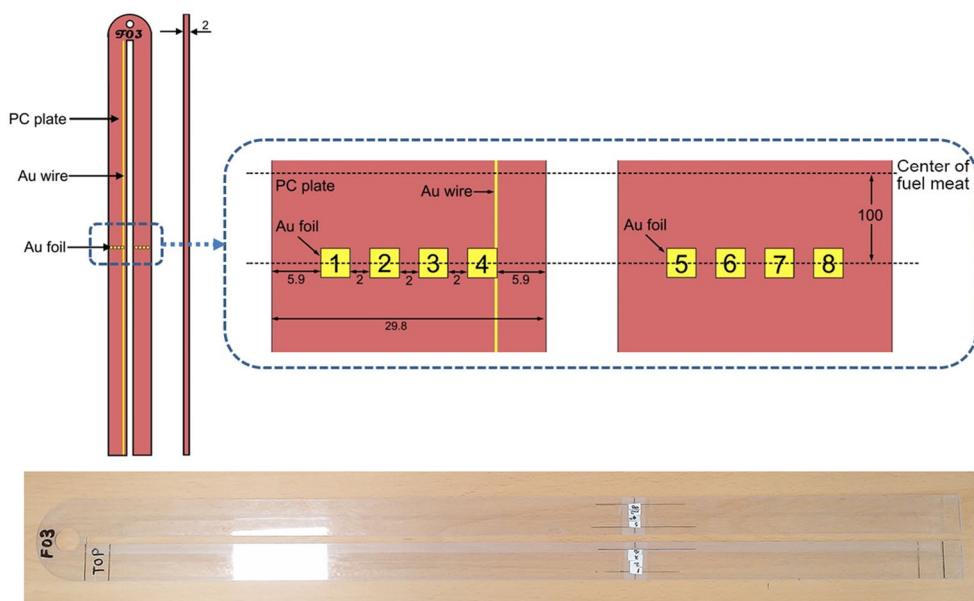
fuel plate has a diameter of 0.1 mm and a length of 64 cm. The Au wire was attached at the one leg of the detector mount with an adhesive plastic tape. The axial position of the Au wire is identical to that of the fuel meat. The Au foil used to measure the transversal neutron flux distribution has a thickness of 0.02 mm and a width and length of about 3 mm. The weight of each Au foil was measured three times and averaged; the weight of a foil sample is about 3 mg. To ensure a simple recovery process, the Au foil was wrapped in 0.01-mm-thick aluminum foil. Eight Au foil specimens were attached between the PC plate. The axial position of the Au foils is -10 cm from the axial center of the fuel meat, where the neutron flux was expected to be the highest. Each PC plate consisted of two plates adhered to each other with the Au wire and foils attached between the two plates.

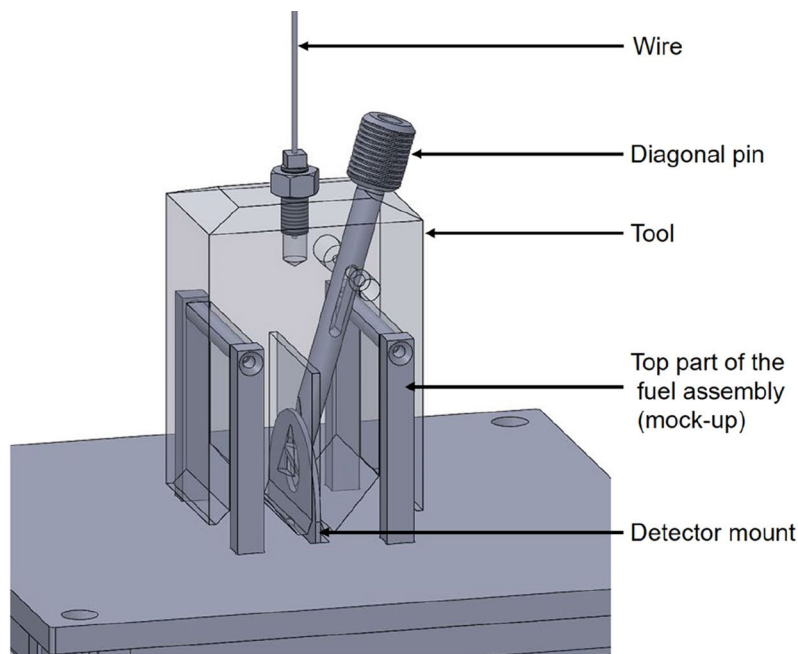Although the flux measurements were conducted at a low reactor power, the irradiated FA cannot be raised to the

Fig. 2 Picture and 3D model of the tool used to withdraw the detector mount from the fuel assembly

reactor pool due to the dose level. Therefore, as shown in Fig. 2, a tool for withdrawing the detector mount from the FA was devised. The tool was developed so as to easily and surely take out the PC plate from the FA. The tool is connected to a long wire and can be lowered to the bottom of the reactor pool with a depth of 10 m. The head of the tool is designed to be fastened to the top part of the FA. While the tool is coupled to the top part of the FA, the diagonal pin of the tool is pushed up as the detector mount moves into the split of the tool. When the tool is fully coupled to the FA, the diagonal pin is caught in the hole of the detector mount.
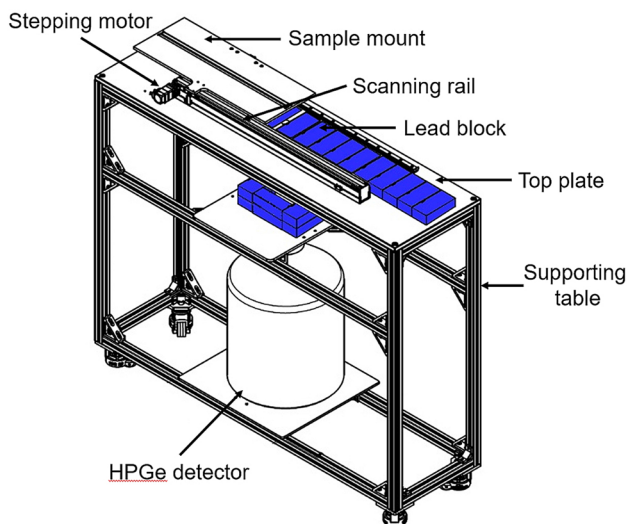
When the tool is pulled up, the detector mount comes out of the FA.

Wire scanning system (WSS)

In order to measure the gamma rays from the long Au wires, an automatic device that moves wires and controls the spectroscopy system was developed. A wire scanning system (WSS) was designed for the wire scanning of activated wire. It is mainly composed of a scanning table, a scanning control module (SCM) and a gamma-ray spectroscopy system. The scanning table consists of a supporting table, a scanning rail, a sample mount, a top plate, a stepping motor, and a lead slit, as shown in Fig. 3. Any type of high-purity germanium (HPGe) detector with a vertical crystal head can be installed in the wire scanning device. The supporting table has one moving axis. Along the scanning rail on the top plate, the sample mount moves in a straight line by means of a stepping motor. Between the top plate and the sample mount, lead blocks are disposed along the scanning rail in order to provide a shield from the gamma rays emitted from the nearby Au wire apart from the measurement position. The scanning width is adjusted by changing the gap between two lead blocks above the detector head. The sample mount has a groove equal in size to one leg of the detector mount, allowing the irradiated detector mount to be installed onto the WSS.

Figure 4a shows images of the SCM. The SCM consists of the motor controller, AC/DC converter, noise filter and the main power circuit. The stepping motor in the WSS is the ORIENTAL AZ series model, and it has a driver package
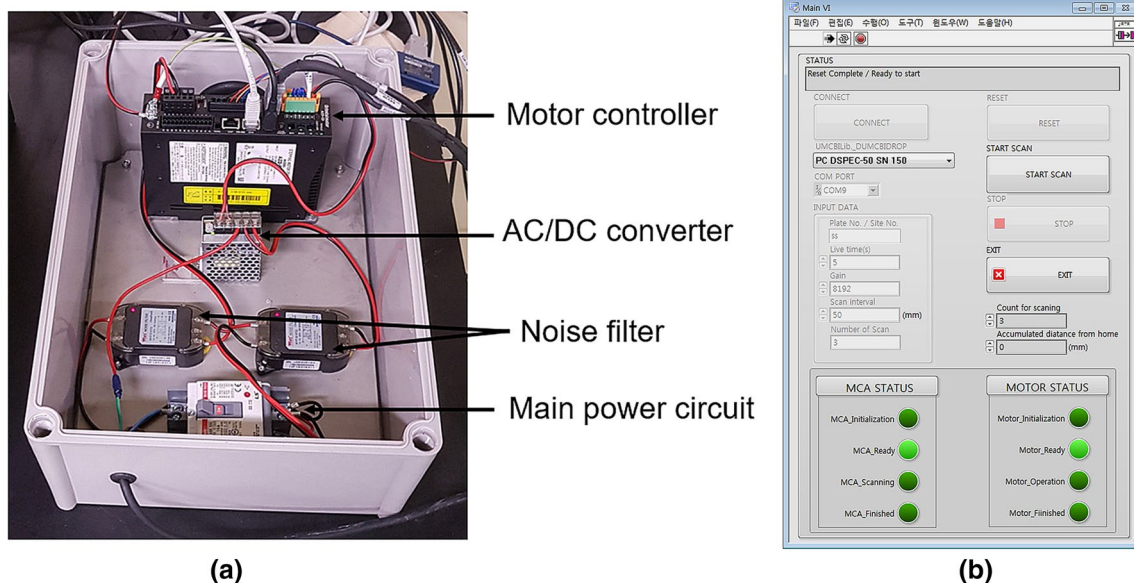

Fig. 3 Wire scanning system

Fig. 4 Components of the scanning control module (**a**) and main window of the wire scanning software (**b**)

with a built-in controller to generate the pulse. In this study, a personal computer was used as the master controller, and the personal computer and the motor controller were connected using a RJ-45/RS-485 to a USB/serial converter. To communicate with the motor controller and to control the multi-channel analyzer (MCA) of the gamma-ray spectroscopy system, wire scanning software was developed. The main code was developed in LabVIEW language to provide a graphic user interface and to run on the MS-Windows platform. The driver was coded to be suitable for the instrument driver development environment provided by National Instruments. For maintenance and for the efficient use of the software driver, the software driver was made of several subVIs (virtual instrument). These VIs are able to connect to each other to realize user-specified processes. The main features of the wire scanning software include a means by which to control the scanning conditions, such as the scanning interval, number of scans and the scanning start position and to control the gamma-ray spectrum measurement conditions such as the counting time and conversion gain in this case. Figure 4b shows the main window of the wire scanning software. An image of the wire scanning system installed at the JRTR site is shown in Fig. 5.

Gamma-ray spectroscopy system

For the gamma-ray spectroscopy system, a closed-end coaxial type HPGe detector with a relative efficiency of 20% is used to measure gamma rays emitted from the irradiated Au wires and Au foils. Figure 6 shows photos of the HPGe detector installed at the WSS and in the low-background shield. The HPGe detector at the WSS was aligned with the scanning slit using the laser pointer. Lead blocks of 5 cm thickness were installed around the detector to shield background gamma rays. For the measurement of gamma rays from Au foils, an ORTEC HPLBS (high-performance, low-background shield) with copper interior shielding was used. Signals generated by the HPGe detector were transmitted and were stored in the memory of the ORTEC DSPEC50 MCA. A personal computer communicated with the MCA through a USB connection and recorded the gamma-ray spectra. An analysis of the acquired spectra was conducted using the wire scanning software.

Using a multi-nuclide standard source made by Eckert & Ziegler Isotope Products, the performance of the gamma-ray spectroscopy system was assessed. A standard gamma-ray source was positioned at a distance of 34 cm from the

Fig. 5 The installed wire scanning system

Fig. 6 HPGe detectors installed in the wire scanning system and in the low-background shield

detector surface, and the measurement time was 38,500 s. The measured full width at half maximum (FWHM) for the 1.33 MeV gamma-ray peak of Co-60 was 1.68 keV. Eight nuclides (Am-241, Cd-109, Co-57, Ce-139, Sn-113, Cs-137, Y-88 and Co-60) were used to determine the absolute full-energy peak efficiency curve. The absolute detection efficiency curve was obtained by the polynomial fitting of log (ε) vs. log (E),

$$\log(\varepsilon) = \sum_{i=0}^{n} c_i \{\log E\}^i, \tag{9}$$

where ε is the absolute efficiency corresponding to the gamma-ray energy E (MeV). In this test, a fourth-order polynomial was used. The as-determined efficiency curve is depicted on a linear scale in Fig. 7 with the fitting uncertainty. The fitted coefficients c_i in Eq. (9) are listed in Table 1. The main source of the uncertainty when determining the absolute detection efficiency comes from the uncertainty of the initial activities of radioactive nuclides in the standard source. All uncertainties of the initial activities were less than 3.2%. In order to compensate the background counts of the gamma-ray spectroscopy system, the background spectrum was measured for 40,000 s of true time. In the background spectrum, there was no net area at 411.8 keV.

Table 1 Fitting coefficients of the detection efficiency function

Coefficient	c_0	c_1	c_2	c_3	c_4
Value	−3.66942	−0.82199	0.11271	−0.59486	−0.96397

Irradiation and measurement

Detector mounts with Au wires and foils were installed at five representative FAs (F03, F04, F10, F12 and F17) among the 18 FAs of the JRTR. Five FAs for the flux measurement were selected to represent assemblies at symmetric positions. A top view of the JRTR core and detector mount installation locations are shown in Fig. 8. The yellow dots on the detector mounts are positions of the Au wires. The zoomed plot of the FA and a side view of the top of the FA are shown in Fig. 9. Each detector mount was inserted into the central coolant channels of the FAs.

After loading the detector mount, the reactor power was increased to 2 kW based on the signals of the ex-core-detectors (wide-range fission chambers) and BF3 counters [10]. Before the power reached 2 kW, the power was increased in a step-wise manner, as shown in Fig. 10. After the reactor power reached 2 kW, the reactor steadily operated for 8 h, and then immediately shut down.

After irradiation, the Au wires and foils were decayed for about 83 h in the reactor pool, after which they were

Fig. 7 Full-energy photopeak efficiency curve of the gamma-ray spectroscopy system

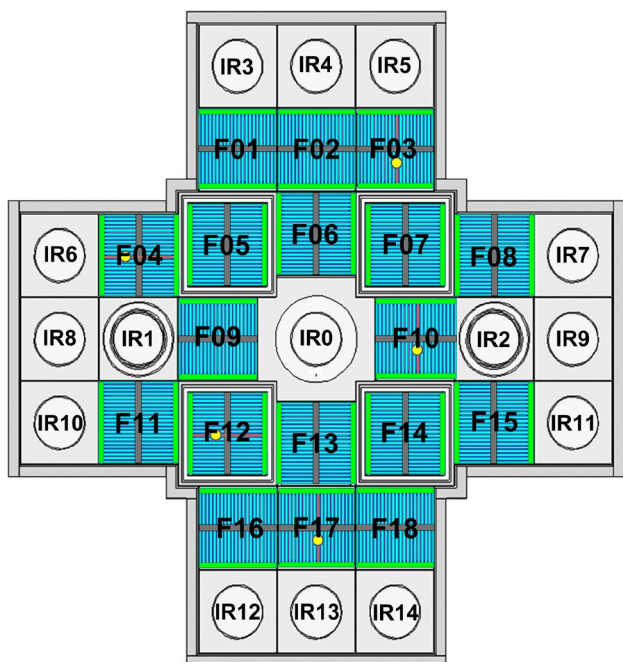**Fig. 8** Locations of the detector mounts and Au wires in the JRTR core (top view)

transferred to the measurement system. Although the irradiated detector mounts were discolored as shown in Fig. 11, the condition of the Au wires and foils was good as they showed no change in location. A PC plate of the detector mount and Au foils were detached, and the remaining PC plate with the Au wire was installed onto the WSS so that the Au wire faced the HPGe detector. Five Au wires were scanned at intervals of 25 mm with a 25 mm slot width. There were 25 scans for one Au wire, and the scan length was 62.5 cm. 0.75 cm each at the top and bottom parts of the Au wire were excluded from the measurements. The measurement time for each scan section was 600 s of live time. Forty Au foils were installed

on the sample mount in the low-background shield. The distance from the surface of the detector to the Au foil was 34 cm. The gamma-ray spectrum of each Au foil was measured for 300 s of live time.

Calculation

In order to determine the neutron flux distribution using the measured reaction rate distribution, the thermal to total reaction rate ratios and the average thermal neutron cross-sections at all measuring points are required. These two factors were obtained by a Monte Carlo simulation for the JRTR. The JRTR core was modeled and reactions of neutrons with Au wires and foils were simulated using the MCNP6 code. Figure 12 shows the MCNP model of the JRTR core. The calculation simulating the experiment was conducted with a core condition nearly identical to that of the experiment. The burnup of fuel before 2 kW operation, exceedingly small, was ignored and fresh fuel was loaded in the calculation model. The control absorber rod (CAR) positions were assumed to be fixed at the corresponding average positions during the experiment. The temperature conditions were considered by adjusting the density of the coolant and the D_2O reflector and by selecting corresponding cross-section data from the ENDF/B-VII.0 nuclear library [11]. The detector mounts were assumed to be at the center of the coolant channel. Au wires with 0.1 mm in diameters and Au foils with 0.02 mm thick were modeled at their corresponding positions. Neutron reaction rates were calculated for each Au foil and at 25 axial segments of each Au wire. To obtain reliable results for these tally regions, enough number of source particles of 9E9 is started to ensure fractional standard deviation of less than 3% for all calculation positions.

Figure 13 shows the calculated thermal to total neutron reaction rate ratio, F for Au foils and wires at each fuel assembly. The values of F are in the range of 0.34–0.64 for all FAs. The energy distribution of neutron in the core
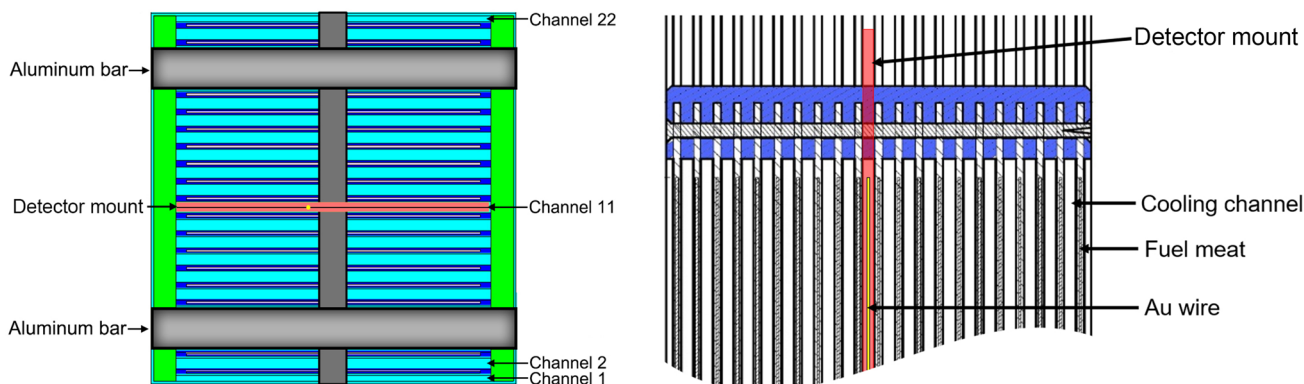

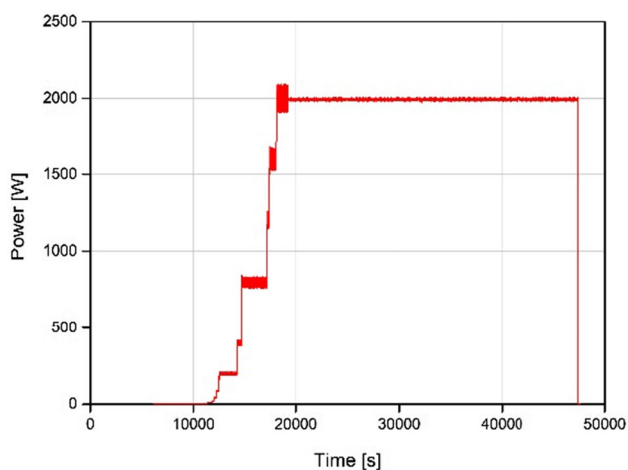**Fig. 9** Position of the detector mount in the fuel assembly

Fig. 10 Power history for the irradiation of the Au wires and foils

relatively large F values due to the Be blocks of IR0 and IR2 on both sides. In contrast, the F values at the F17, which has an irradiation hole on one side, are small. Since the core of JRTR is compact and has a complex structure with reflector material inside the core, the value of F varies with position. The distributions of the F for Au foils and wires indicate the transversal and axial energy distribution of neutrons in each fuel assembly. In both the transversal and axial directions, the value of F tends to increase toward both ends of the fuel plate. The uncertainties of the F are in the range of 1.81–2.94% for Au foils and 1.64–7.91% for Au wires, respectively. The difference in uncertainty of F at the Au wire is large, because the number of neutrons reaching both ends of the wire is relatively small, resulting in a large statistical error in the calculation of the reaction rate.

depends on nearby structural materials such as beryllium (Be) blocks surrounding the vertical irradiation holes and the D_2O reflectors outside the fuel assemblies. The F10 has
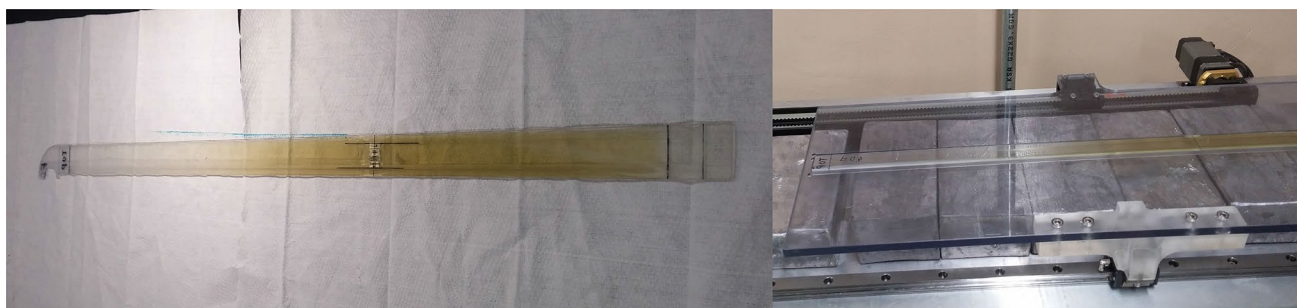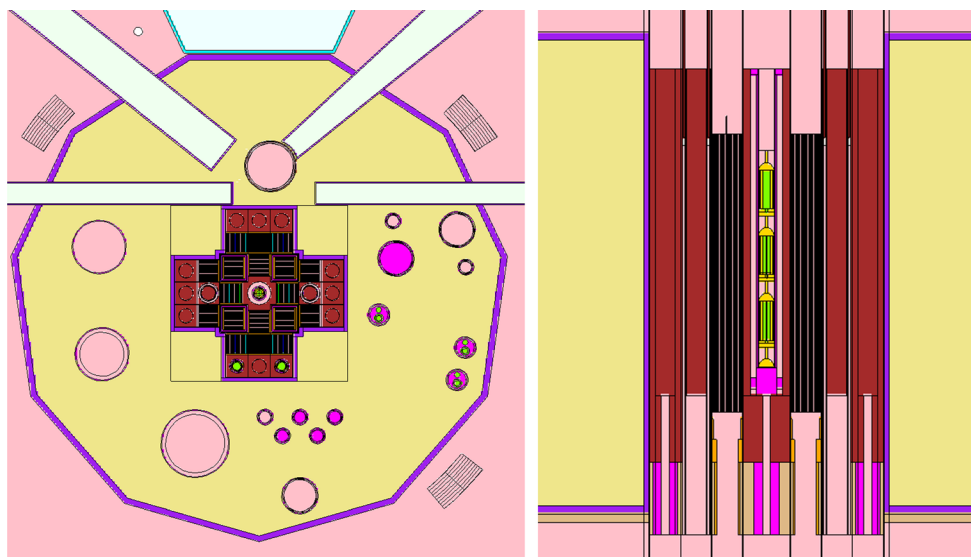

Fig. 11 Images of an irradiated detector mount and a PC plate loaded on the wire scanning system

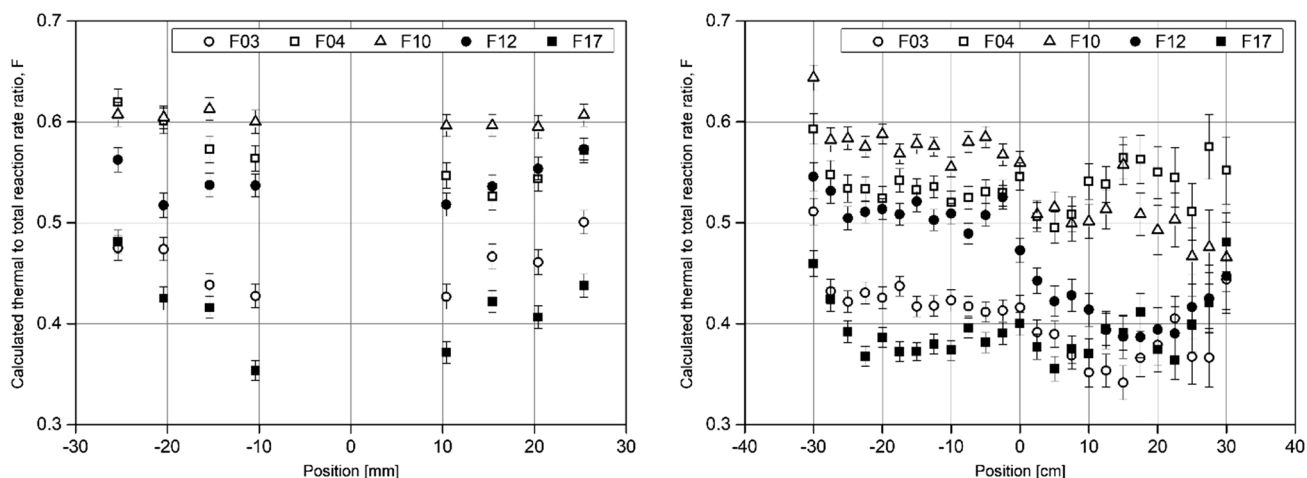**Fig. 12** MCNP calculation model for the JRTR core

Fig. 13 Calculated thermal to total reaction rate ratio, F for Au foils (left) and Au wires (right)
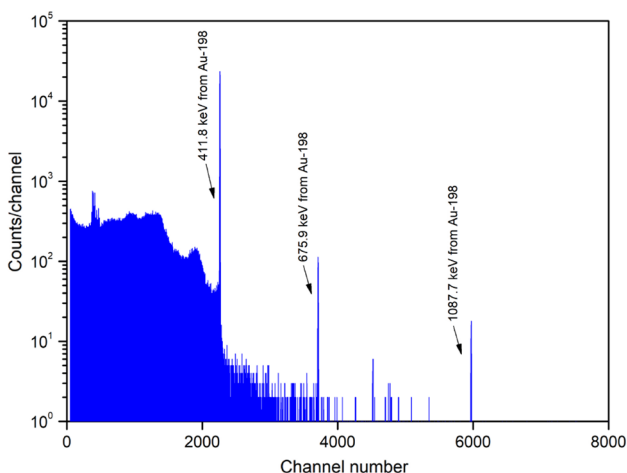

Fig. 14 Gamma-ray energy spectrum of an Au foil specimen irradiated in fuel assembly F03

Results and discussion

Using the gamma-ray spectra of 40 Au foils, the reaction rate of Au-197 was determined and the fission power of the reactor was evaluated. Au foils were irradiated at 2 kW by the neutron measurement systems initially calibrated at around 10 μW by neutron noise analysis [8]. As it was the first power rise to the kW range, this experiment intended the second power calibration as well at around 2 kW.

Figure 14 shows the measured gamma-ray spectrum of the Au foil installed at the edge of the F03 FA (F03-01). In the figure, the main peak at 411.8 keV (Iγ = 95.62%) and minor peaks at 675.9 keV (Iγ = 0.805%) and 1087.7 keV (Iγ = 0.1589%) can be observed [13].

For the measurement of the activity of Au-198, the peak at 411.8 keV was used. The activity of Au-198 at the end of the irradiation process is determined by Eq. (5), and using this value, the reaction rate under 2 kW operation is determined. During the calculation of the reaction rate, the power history during irradiation is considered. From Fig. 10, the Au wires and foils are assumed to be irradiated in the reactor core in six stages – 200 W (t_0–t_1), 400 W (t_1–t_2), 800 W (t_2–t_3), 1200 W (t_3-t_4), 1600 W (t_4–t_5), and 2 kW (t_5–t_6). t_0 is the start time of 200 W and t_6 is the shutdown time. The time elapsed during the power rise was neglected because each rising time was less than few minutes. The total neutron capture reaction rate R can be derived from Eq. (3), as follows,

$$R = \frac{A(t_i)}{1 - e^{-\lambda t_i}}. \tag{10}$$

If $t_0 = 0$, the power rises at time t_1, t_2, t_3, …; the power reaches 2 kW at t_{n-1} and shutdown occurs at t_n. In this case, the reaction rate at 2 kW of reactor power R_0 becomes.

$$R_0 = \frac{A(t_n)}{e^{-\lambda t_n} \sum_{i=1}^{n} \left[a_i (e^{\lambda t_i} - e^{\lambda t_{i-1}}) \right]}, \tag{11}$$

where a_i denotes the relative power level in comparison with 2 kW, i.e.:

$$a_i = \frac{\text{reactor power at time } t_{i-1}}{2\,\text{kW}} \tag{12}$$

The total reaction rate of 40 Au foils are between 2.097E7 and 3.895E7 reaction/s. The measured reaction rates of the Au foils and the MCNP calculation results are compared in Fig. 15. In the figure, the x axis is the total reaction rate per 1 g of Au foil as calculated by the MCNP for 2 kW of power, and the y axis is the measurement result. In the linear fitting,
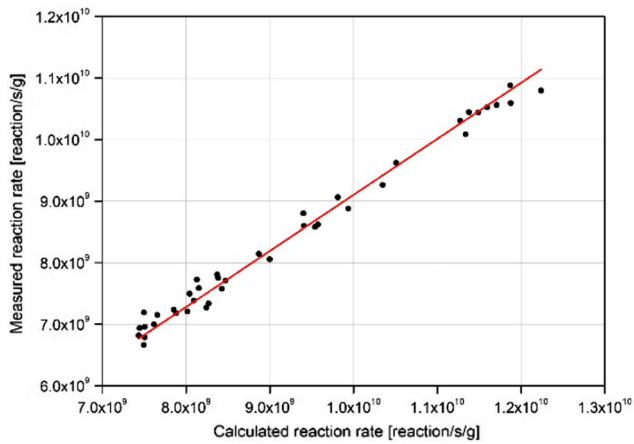
Fig. 15 Least square fitting between the measured and calculated reactions rates of 40 Au foils (calculated reaction rates are at 2 kW)

Fig. 17 Least square fitting between the measured and calculated reactions rates of 125 segments of Au wires

the fitted slope of 0.910105 means that the actual power is approximately 9% lower than 2 kW. Therefore, in this study, the actual reactor power can be assumed to be 1.820 kW. Although there are some deviations, it can be seen that the calculation result and the measurement result follow the fitted line well.

Figure 16 shows measured and calculated reaction rate distributions in the cooling channels along with the transversal directions of each FA. The x-axis is the position of the Au foil when the transversal center of the fuel is 0. The reaction rates tend to be low in the middle and high at both ends for all FAs. The measurement results are in good agreement with the simulation results. The largest difference between the measurement and the calculation of the averaged reaction rate for each FA is found at the F17 FA, which is 1.32%.

As the weight of the Au wire corresponding to each slot width cannot be accurately determined, only the relative reaction rate distribution along the axial direction at each
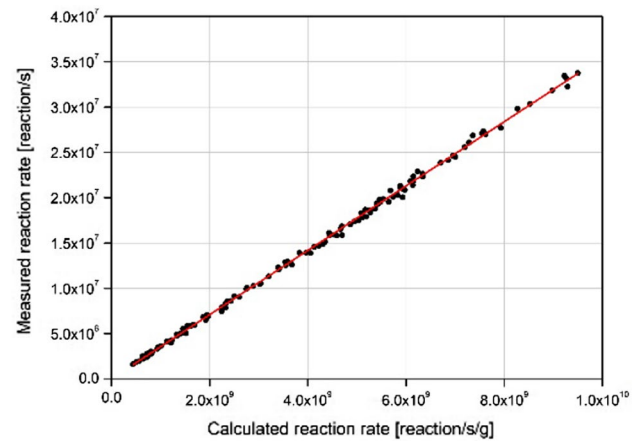
FA can be obtained from the result of the Au wire scanning. Therefore, as shown in Fig. 17, the MCNP result (total reaction rate per 1 g of Au wire) and the measurement result (total reaction rate per 2.5 cm slot width of Au wire) are linearly fitted. The fitted slope of 3.547E-3 is used as a factor to convert the measured relative reaction rate into the absolute value. In the figure, an excellent proportionality between the measurement and the simulation is shown.

Figure 18 shows the measured and calculated axial reaction rate distributions of the Au wires at each FA. The x-axis is the axial position of the Au wire when the axial center of the fuel is 0. For all five FAs, the distribution is shifted downward with a peak position at around -15 cm from the center of the fuel, which is due to CARs at the core upper region during the irradiation. The measured and simulated results show excellent agreements. The largest difference
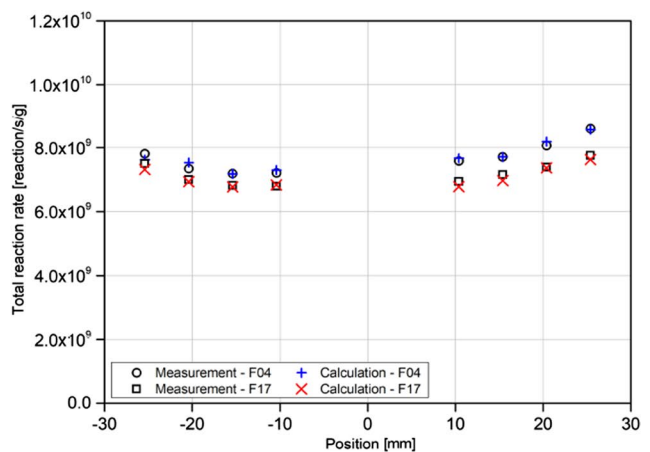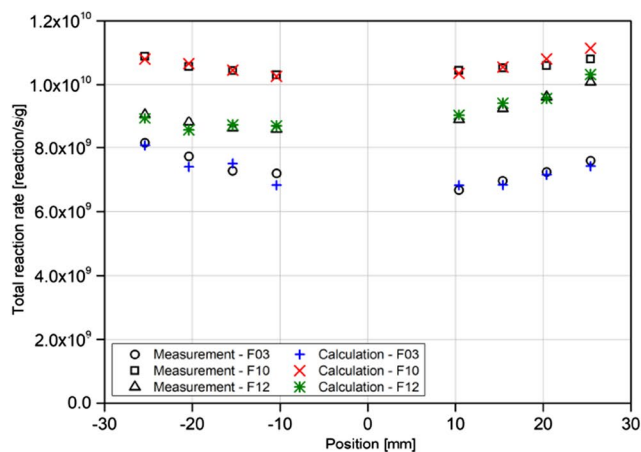

Fig. 16 Measured and calculated reaction rate distributions along with the transversal direction of the fuel assembly
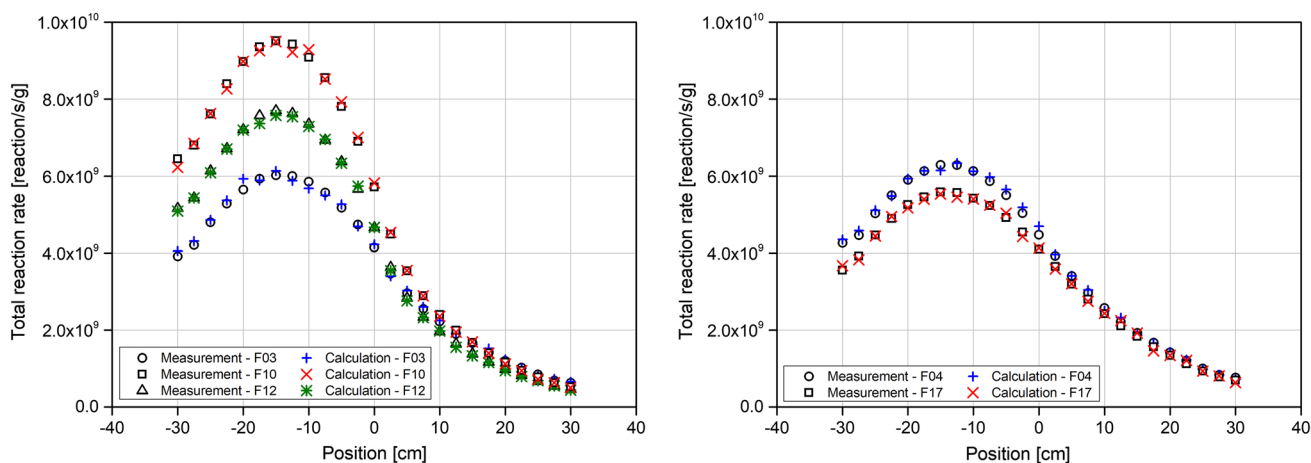
Fig. 18 Measured and calculated reaction rate distributions along the axial direction of the fuel assembly

between the measured and simulated values with regard to the averaged reaction rate for each FA is 0.93% at F12.

From the Eqs. (7) and (8), the thermal neutron flux distribution is determined using the total reaction rate distribution of the Au foils. The fractions of the thermal neutron reaction in the total reaction and average cross-section of the thermal (≤ 0.625 eV) neutrons were calculated by MCNP simulations. The neutron self-shielding effect due to the thickness

of the Au foil is considered to determine the neutron flux in the absence of Au foil. It is assumed that the Au foil is irradiated by isotropic neutrons with velocity of 2200 m/s. The calculated value of the thermal neutron self-shielding factor for 0.02-mm-thick Au foil is 0.982 [13]. Table 2 lists the estimated measured total reaction rate at a reactor power of 1.820 kW and thermal neutron flux per unit power.

Table 2 Measured total reaction rate and thermal neutron flux at each fuel assembly

Irradiation position	Measured total reaction rate at 1.820 kW (reaction/s/g)	Thermal to total reaction rate ratio, F	Thermal neutron flux per unit power [#/cm²s/kW]	Irradiation position	Measured total reaction rate at 1.820 kW (reaction/s/g)	Thermal to total reaction rate ratio, F	Thermal neutron flux per unit power [#/cm²s/kW]
F03-01	8.144E9	0.475	9.892E09	F10-05	1.044E10	0.596	1.501E10
F03-02	7.725E9	0.474	9.541E09	F10-06	1.052E10	0.596	1.520E10
F03-03	7.269E9	0.439	8.374E09	F10-07	1.059E10	0.595	1.516E10
F03-04	7.192E9	0.428	8.168E09	F10-08	1.080E10	0.607	1.567E10
F03-05	6.663E9	0.427	7.483E09	F12-01	9.060E9	0.562	1.252E10
F03-06	6.959E9	0.466	8.509E09	F12-02	8.799E9	0.517	1.126E10
F03-07	7.232E9	0.461	8.598E09	F12-03	8.619E9	0.537	1.164E10
F03-08	7.588E9	0.501	9.567E09	F12-04	8.578E9	0.537	1.155E10
F04-01	7.807E9	0.619	1.158E10	F12-05	8.878E9	0.518	1.153E10
F04-02	7.337E9	0.601	1.069E10	F12-06	9.259E9	0.536	1.230E10
F04-03	7.180E9	0.573	1.009E10	F12-07	9.618E9	0.554	1.313E10
F04-04	7.206E9	0.564	1.007E10	F12-08	1.009E10	0.573	1.416E10
F04-05	7.578E9	0.547	1.031E10	F17-01	7.496E9	0.481	9.423E09
F04-06	7.710E9	0.526	1.002E10	F17-02	6.998E9	0.425	7.887E09
F04-07	8.059E9	0.543	1.082E10	F17-03	6.815E9	0.416	7.585E09
F04-08	8.596E9	0.572	1.212E10	F17-04	6.788E9	0.354	6.669E09
F10-01	1.088E10	0.607	1.577E10	F17-05	6.938E9	0.372	7.024E09
F10-02	1.056E10	0.605	1.550E10	F17-06	7.154E9	0.422	8.239E09
F10-03	1.044E10	0.613	1.545E10	F17-07	7.382E9	0.407	8.040E09
F10-04	1.031E+10	0.600	1.494E10	F17-08	7.751E9	0.438	9.009E09

The average fractional standard deviation of the simulation results for 165 reaction rates in the FAs (125 points of Au wire scanning and 40 points of Au foils) was 2.365%. The uncertainty of the measurement data originates from uncertainties in the position of neutron irradiation, the weight of the Au foil, the counting statistics, the counting geometry, the straightness of the Au wire, the uniformity of the Au wire, and nuclear data, among other sources. The experiment was carefully designed and implemented to minimize these uncertainty sources. The uncertainty of the weight of the Au foil was 0.001 mg when foil weight was in the range of 2.91–3.82 mg. The average value of this uncertainty was 0.03% for 40 Au foils. The uncertainty of the initial activity of the standard gamma-ray source for the efficiency calibration is 3.2%, which is somewhat large compared to other uncertainties. The uncertainty of the counting statistics is in the range of 0.15–0.7% for all 165 measured data instances. Other uncertainties are difficult to quantify and were assumed to be negligible. The total uncertainty of the measurement results is in the range of 3.66–4.61%.

Conclusions

In this work, the neutron reaction rate distribution in the fuel assemblies of a research reactor was measured to check the reliability of predictions of the power distribution at around 2 kW of reactor power and to provide basic data to ensure reliable reactor operation. As a result, the reactor power during irradiation was found to be approximately 9% lower than indications of NMS which initially calibrated at around 10 μW based on neutron noise analyses. This proves that the linearity of the NMS indications had been well maintained even when the reactor power was increased by eight decades from 10 μW to 2 kW. For five fuel assemblies, the thermal neutron flux per unit power is in the range of 6.669E9–1.567E10 n/cm^{2}s/kW at measured points. The differences between the measurement and calculation of the averaged reaction rate for each FA are within 1.32% and 0.93% in the transversal direction and in the axial direction of the fuel assembly, respectively. From these results, it is confirmed that the neutron flux measurement of the JRTR was successfully performed and that the MCNP model of the core suitably predicts the spatial profile of the flux and power distribution. The JRTR is the first case of using Monte Carlo code for nuclear design, and the reliability of the design can be confirmed through the results of this study.

References

1. IAEA-TECDOC-1234: The applications of research reactors (2001) Report of an Advisory Group meeting held in Vienna, 4–7 October 1999
2. Neutron fluence measurements (1970) Technical reports series No.107, International Atomic Energy Agency 1970
3. Radulović V, Štancar Ž, Snoj L, Trkov A (2014) Validation of absolute axial neutron flux distribution calculations with MCNP with ^{197}Au(n, γ)^{198}Au reaction rate distribution measurements at the JSI TRIGA MarkII reactor. Appl Radiat Isotopes 84:57–65
4. Chiesa D, Clemenza M, Nastasi M, Pozzi S, Previtali E, Scionti G, Sisti M, Prata M, Salvini A, Cammi A (2015) Measurement and simulation of the neutron flux distribution in the TRIGA Mark II reactor core. Ann Nucl Energy 85:925–936
5. Molina F, Aguilera P, Romero-Barrientos J, Arellano HF, Agramunt J, Medel J, Morales JR, Zambra M (2017) Energy distribution of the neutron flux measurements at the Chilean Reactor RECH-1 using multi-foil neutron activation and the expectation maximization unfolding algorithm. Appl Radiat Isotopes 129:28–34
6. Kim KO, Jun BJ, Lee B, Park SJ, Roh G (2020) Comparison of first criticality prediction and experiment of the Jordan research and training reactor (JRTR). Nucl Eng and Tech 52:14–18
7. Park J, Son HM, Song K, Altamimi RM (2020) Measurement of core flow distribution in a research reactor using plate-type fuel assembly. Ann Nucl Energy 148:107750
8. Park B, Jun BJ, Yoo H, Lee B, Park SJ, Roh G, Khafaji S (2019) Measurement of kinetic parameter of the Jordan research and training reactor. Ann Nucl Energy 132:322–326
9. Suaifan M, Kahook SD, Almomani S, Seong BS (2018) Status and perspectives on the utilization of a new nuclear research reactor in Jordan. Phys B 551:431–435
10. Bae S, Suh S, Cha H (2017) Assessment of the implementation of a neutron measurement system during the commissioning of the jordan research and training reactor. Nucl Eng Tech 49:504–516
11. MacFarlane RE, Kahler AC (2010) Methods for processing ENDF/B-VII with NJOY. Nucl Data Sheets 111:2739–2890
12. National Nuclear Data Center, Brookhaven National Laboratory, "Nudat2.8". www.nndc.bnl.gov/nudat2/
13. Martinho E, Salgado J, Gonçalves IF (2004) Universal curve of the thermal neutron self-shielding factor in foils, wires, spheres and cylinders. J Radioanal Nucl Chem 261:637–643